Enhanced mass transport in ultrarapidly heated Ni/Si thin-film multilayers

L. P. Cook,[1,2] R. E. Cavicchi,[1,a)] N. Bassim,[1,3] S. Eustis,[1,4] W. Wong-Ng,[1] I. Levin,[1]
U. R. Kattner,[1] C. E. Campbell,[1] C. B. Montgomery,[1] W. F. Egelhoff,[1] and M. D. Vaudin[1]
[1]*National Institute of Standards and Technology, Gaithersburg, Maryland 20899, USA*
[2]*PhazePro Technologies, LLC, Hustontown, Pennsylvania 17229, USA*
[3]*Naval Research Laboratory, Washington, D.C. 20375, USA*
[4]*Directed Vapor Technologies International, Inc., Charlottesville, Virginia 22903, USA*

(Received 21 July 2009; accepted 28 September 2009; published online 23 November 2009)

We investigated multilayer and bilayer Ni/Si thin films by nanodifferential scanning calorimetry (nano-DSC) at ultrarapid scan rates, in a temperature-time regime not accessible with conventional apparatus. DSC experiments were completed at slower scan rates as well, where it was possible to conduct parallel rapid thermal annealing experiments for comparison. Postexperimental characterization was accomplished by x-ray diffraction, and by transmission electron microscopy (TEM) and energy-filtered TEM of thin cross sections prepared by focused ion beam milling. We found that rate of heating has a profound effect on the resulting microstructure, as well as on the DSC signal. After heating to 560 °C at 120 °C/s, the general microstructure of the multilayer was preserved, in spite of extensive interdiffusion of Ni and Si. By contrast, after heating to 560 °C at 16 000 °C/s, the multilayer films were completely homogeneous with no evidence of the original multilayer microstructure. For the slower scan rates, we interpret the results as indicating a solid state diffusion-nucleation-growth process. At the higher scan rates, we suggest that the temperature increased so rapidly that a metastable liquid was first formed, resulting in complete intermixing of the multilayer, followed by crystallization to form solid phases. The integrated DSC enthalpies for both multilayer and bilayer films are consistent with this interpretation, which is further supported by thermodynamic predictions of metastable Ni/Si melting and solid state Ni/Si interdiffusion. Our results suggest that use of heating rates >10 000 °C/s may open new avenues for intermetallic micro- and nanofabrication, at temperatures well below those prevailing during explosive silicidation. © *2009 American Institute of Physics*. [doi:10.1063/1.3254225]

I. INTRODUCTION

As the technology for complementary metal oxide semiconductor (CMOS) devices advances to feature sizes of 28 nm and below, replacement of the polysilicon/SiO_2 gate stack combination represents a key paradigm shift. The industry is moving toward a metal gate/high-κ dielectric combination in which fully silicided metal gates are receiving a lot of attention as candidates for the metal layer.[1–6] An important example is the Ni–Si system which consists of a number of phases with optimal electrical conductivity and work function.[2] In developing this technology, the thermal stability, and thermal compatibility with other CMOS processes are important factors.[1] The use of ultrarapid thermal annealing processes which occur on the millisecond time scale are being investigated for the control of dopant distributions in ultrashallow junctions.[7,8] It has also recently been demonstrated that the Ni–Si reaction can occur using laser annealing[9,10] and such ultrafast processing of Ni–Si represents an important avenue for continuing Moore's law progression.[11] While it seems clear that the processes of diffusion and reaction that are responsible for forming the silicides will have different kinetics, the effect of ramp rate on the reactions remains unexplored.

The Ni–Si reaction has been previously studied with Ni deposited on single crystal Si,[5] polysilicon,[6] and for cosputtered Ni and Si.[4] During reaction, more than one phase may be present, for example, in the work of Rivero *et al.*,[5] the reaction proceeded via a mixture of Ni_2Si and Ni_3Si_2 for a 13 nm Ni patch deposited on a single crystal. In experiments with Ni on polysilicon,[6] it was found that the ratio of the thicknesses of deposited Ni and Si determined the composition of the silicide, with intermediate silicides of NiSi and $Ni_{31}Si_{12}$ formed during the anneal. Cosputtering the two materials also allowed control of composition and was shown to affect the work function.[4] Calorimetric measurements have proven useful at elucidating the processes during a Ni–Si reaction,[12] as have detailed kinetic studies.[13]

It was the aim of this study to explore the Ni–Si reaction at rapid heating rates using a combinatorial approach with a microelectromechanical device that allowed for simultaneous heating and differential scanning calorimetry (DSC) measurements. By comparing postreaction characterization results for a bilayer with a multilayer of Ni–Si, each with the same total thickness, we were able to investigate the role of interdiffusion. As expected, the reaction was enhanced in the multilayer sample due to a short diffusion distance. The surprising finding is that there is a strong enhancement of Ni/Si mixing with rapid ramp rate.

II. EXPERIMENTAL PROCEDURE

The nanocalorimeter shown in Fig. 1 acts like a miniature differential scanning calorimeter.[14] The device consists of a $66 \times 240 \times 3.3\ \mu m^3$ thick inner suspended platform divided into sample and reference zones. The device was fab-

[a)]Electronic mail: rcavicchi@nist.gov.

 © 2009 American Institute of Physics

Downloaded 24 Nov 2009 to 132.250.22.8. Redistribution subject to AIP license or copyright; see http://jap.aip.org/jap/copyright.jsp

Report Documentation Page

Form Approved OMB No. 0704-0188

Public reporting burden for the collection of information is estimated to average 1 hour per response, including the time for reviewing instructions, searching existing data sources, gathering and maintaining the data needed, and completing and reviewing the collection of information. Send comments regarding this burden estimate or any other aspect of this collection of information, including suggestions for reducing this burden, to Washington Headquarters Services, Directorate for Information Operations and Reports, 1215 Jefferson Davis Highway, Suite 1204, Arlington VA 22202-4302. Respondents should be aware that notwithstanding any other provision of law, no person shall be subject to a penalty for failing to comply with a collection of information if it does not display a currently valid OMB control number.

1. REPORT DATE	2. REPORT TYPE	3. DATES COVERED
2009		**00-00-2009 to 00-00-2009**

4. TITLE AND SUBTITLE **Enhanced Mass Transport in Ultrarapidly Heated Ni/Si Thin-Film Multilayers**	5a. CONTRACT NUMBER 5b. GRANT NUMBER 5c. PROGRAM ELEMENT NUMBER
6. AUTHOR(S)	5d. PROJECT NUMBER 5e. TASK NUMBER 5f. WORK UNIT NUMBER
7. PERFORMING ORGANIZATION NAME(S) AND ADDRESS(ES) **National Institute of Standards and Technolog,Gaithersburg,MD,20899**	8. PERFORMING ORGANIZATION REPORT NUMBER
9. SPONSORING/MONITORING AGENCY NAME(S) AND ADDRESS(ES)	10. SPONSOR/MONITOR'S ACRONYM(S) 11. SPONSOR/MONITOR'S REPORT NUMBER(S)

12. DISTRIBUTION/AVAILABILITY STATEMENT

Approved for public release; distribution unlimited

13. SUPPLEMENTARY NOTES

14. ABSTRACT

15. SUBJECT TERMS

16. SECURITY CLASSIFICATION OF:			17. LIMITATION OF ABSTRACT	18. NUMBER OF PAGES	19a. NAME OF RESPONSIBLE PERSON
a. REPORT	b. ABSTRACT	c. THIS PAGE			
unclassified	**unclassified**	**unclassified**	**Same as Report (SAR)**	**6**	

Standard Form 298 (Rev. 8-98)
Prescribed by ANSI Std Z39-18

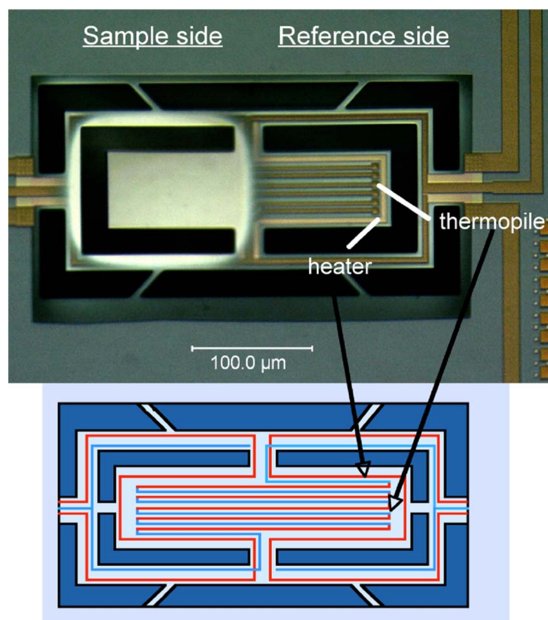

FIG. 1. (Color online) Photomicrograph and schematic of nanocalorimeter.

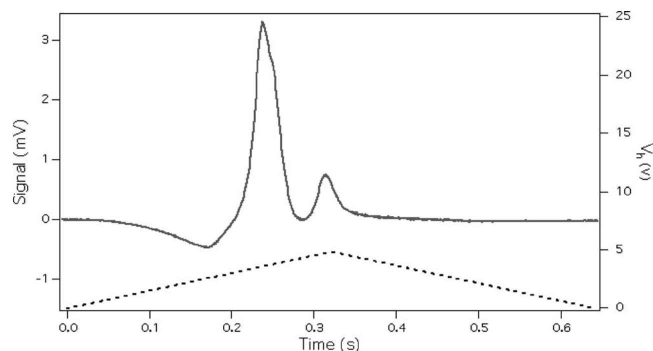

FIG. 2. DSC signal and heater voltage vs time for 2000 °C/s ramp rate for the multilayer sample.

ricated in an array of six elements. Films are deposited on the sample side using a shadow mask. Each zone has an integral poly-Si heater and an Al/poly-Si thermopile for measuring the temperature difference between the two zones. To enhance the thermal isolation of the inner platform, the leads to the thermopile and heater run along a suspended platform that surrounds the inner platform. Chips are mounted in packages and placed in a high vacuum system for calorimetry scans. The thermopile produces a signal of 1.8 mV/K that yields 1 mK resolution at a 10 kHz bandwidth. During a scan, separate heater voltage (V_h) ramps were applied to the sample and reference heaters, and the thermopile signal was recorded using a preamplifier and digital oscilloscope. A set of devices coated with melting point standards (In, Sn, Pb, Al–Ge eutectic) was produced to calibrate temperature and enthalpy for each of the ramp rates used in the Ni–Si measurements. DSC scans consisted of a ramp up to a maximum temperature, followed immediately by a ramp down to room temperature. This sequence was repeated until there was no change in the signal from one scan to the next. The signal from the last scan (which was due to differences in the heat capacity of the reacted sample and the reference side) was used as a baseline, which was subtracted from the earlier scans, to provide difference scans showing the progression of the Ni/Si reaction.

Films of Si and Ni were deposited on the nanocalorimeters by magnetron sputtering at a base pressure of 2.7×10^{-6} Pa. Two sets of samples were prepared with the total Ni and Si content the same for the two sets. Bilayer samples consisted of layers of 100 nm Ni and 100 nm Si, and the multilayer films were composed of ten sequences of (10 nm Ni/10 nm Si). Films on test coupons of Si wafers coated with 500 nm of thermal oxide were prepared simultaneously for use in parallel RTA experiments. Postexperimental characterization utilized x-ray diffraction (XRD), focused ion-beam milling and transmission electron microscopy (FIB/TEM), scanning electron microscopy with energy dispersive x-ray analysis, and reflected light microscopy.

Samples for TEM from individual devices were cut and thinned using FIB methods. Compositional mapping was accomplished using energy-filtered TEM (EFTEM) in a JEOL 3010 ultra-high resolution (UHR) TEM (300 kV) equipped with a Gatan imaging filter.[15] The Si $L_{2,3}$ edge, Ni $M_{2,3}$, and Ni $L_{2,3}$ absorption edges were used. A three-window method was used to isolate the signal from the background. Partial overlap of the Ni $M_{2,3}$ (65 eV) and Si (100 eV) edges precludes accurate background subtraction under the Si $L_{2,3}$ edge; however, semiquantitative analyses are still possible.

III. RESULTS

A. Differential scanning calorimetry

A representative DSC scan of a multilayer sample is shown in Fig. 2, where we plot a difference scan for an intermediate heating rate of 2000 °C/s. The main features of this scan are a relatively large exothermic peak (referred to as peak 1) initiating at a heater voltage (V_h) of 2.55 V (corresponding to 234 °C), followed by a smaller exothermic effect (peak 2) starting at 4.28 V (483 °C). We interpret these effects as originating from Ni/Si reactions activated at different temperatures. The later exothermic effect continues beyond the maximum heater voltage into the cooling part of the cycle. These effects are greatly diminished in scans beyond the first, indicating that reaction was nearly complete after the first scan.

In Fig. 3, we show a series of five DSC scans at different rates. A normalization was used for each scan so that the signals may be conveniently compared, as the raw signal versus time traces differ significantly both in duration and amplitude. The signal amplitudes for each scan rate were normalized by the respective scan rate, and the abscissa shows time divided by total scan time. This ratio is the fraction of scan completed. Also shown is $V_h/V_{h\,max}$, where $V_{h\,max}$ is the maximum heater voltage. The horizontal offset of each DSC scan is adjusted so that all $V_h/V_{h\,max}$ plots coincide. Figure 3 shows an interesting evolution in the fine structure of the DSC peaks as the scan rate is increased. At 490 °C/s, peak 1 shows double maxima, the higher voltage (higher temperature) one of which gradually diminishes with increasing scan rate, until no longer distinguishable at

Downloaded 24 Nov 2009 to 132.250.22.8. Redistribution subject to AIP license or copyright; see http://jap.aip.org/jap/copyright.jsp

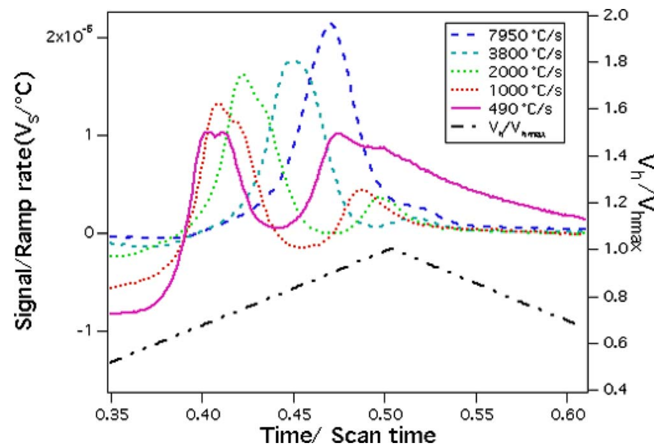

FIG. 3. (Color online) DSC signal divided by the scan rate for five scan rates plotted against normalized scan time. Also shown is the normalized applied heater voltage V_h.

7950 °C/s. As discussed below, this feature may indicate added complexity in the reaction represented by peak 1.

By integrating the areas under the two peaks defined in Fig. 2, it is possible to get an estimate of the enthalpy of reaction as a function of scan rate by reference to the Al/Ge eutectic data mentioned above. Results are shown in Fig. 4, where the inset indicates the variation of the areas for peak 1 and peak 2 as a function of scan rate. Note that peak 1 decreases from its maximum at the slowest scan rate to nearly zero at the highest scan rate, whereas peak 2 shows the reverse trend. The sums of the two peak areas show a monotonic increase with scan rate, suggesting either that enthalpy production and completion of reaction are enhanced at high scan rates, or that differential heat loss is greater at the slow scan rates. For comparison we also show in Fig. 4 the cumulative results of similar experiments on a Ni/Si bilayer. Although the data are less extensive, a similar trend is evident for the bilayer.

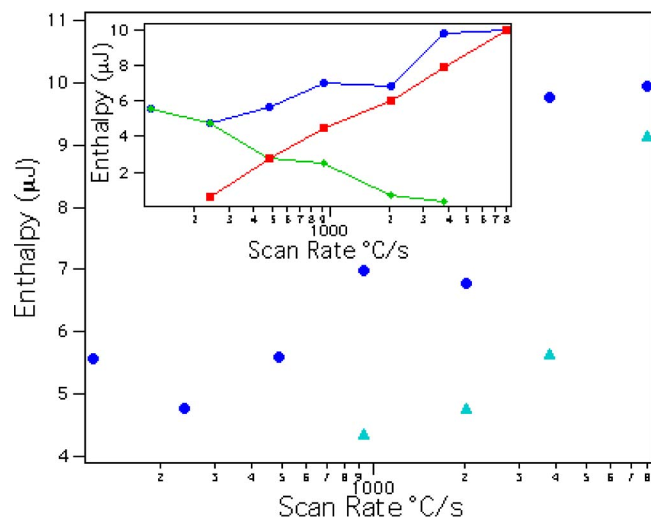

FIG. 4. (Color online) Sum of peak area (enthalpy) vs scan rate for multilayer (circles) and bilayer (solid triangles). Inset: peak 1 enthalpy (diamonds), peak 2 enthalpy (squares), and sum of peak areas (circles) vs scan rate for multilayer sample.

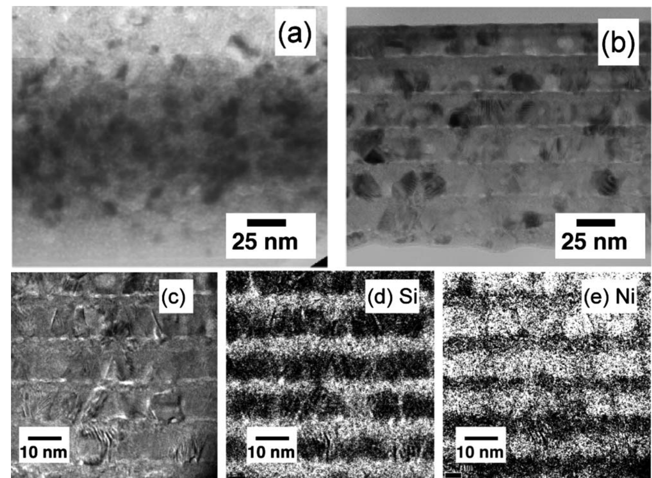

FIG. 5. TEM images from Ni/Si multilayer sample annealed with a ramp rate of (a) 16 000 °C/s and [(b)–(e)] 120 °C/s. (c) Magnified brightfield image. [(d) and (e)] EFTEM maps for Si and Ni from the same area.

B. Postexperimental characterization

In Figs. 5(a) and 5(b) we show microstructures of the rapidly scanned versus slowly scanned multilayered films, as obtained by TEM bright field imaging. A large difference is obvious, in that the rapidly scanned material [Fig. 5(a)] is essentially homogeneous, whereas the slow scan [Fig. 5(b)] retains a multilayered structure. This is further borne out by the energy-filtered (EFTEM) compositional maps of Fig. 5(d) (Si) and Fig. 5(e) (Ni), which show a layered heterostructure of alternating Si- and Ni-rich layers. Detailed analysis of the EFTEM spectra for the slow scan showed that substantial interdiffusion of Ni and Si occurred, resulting in relatively homogeneous bilayers of stoichiometrically distinct Ni-silicides. In Figs. 5(b) and 5(c), thin, discontinuous areas with high signal (bright) are evident at every other Ni/Si junction. These small areas have the highest Si concentration and are comprised of a third, Si-rich phase. By contrast with the slowly scanned material of Fig. 5(b), EFTEM data for the rapidly scanned sample in Fig. 5(a) were featureless and showed no discernible compositional layering; the sample appeared to have become homogeneous with regard to Ni and Si distribution. Due to the partial overlap of Ni and Si edges, quantitative information on phase compositions was not obtained for the slowly scanned material.

Information on identity of crystalline phases in the reacted Ni/Si multilayers was obtained from two sources: (1) selected area electron diffraction (SAED) data taken from FIB samples of the DSC sensors and (2) XRD data on multilayered coupons subjected to a rapid thermal anneal at 50 °C/s. Data from the two sources are consistent in that the principal phases identified are Ni_3Si (major), (Ni,Si) solid solution, $NiSi_2$ (major), and Si. No measurable difference was observed between the SAED patterns from sections of the slow scanned and the rapidly scanned DSC samples.

IV. DISCUSSION

A. Generalized interpretation

Based on examination of the combined TEM, EFTEM, SAED, XRD, and DSC data, we developed working hypoth-

Downloaded 24 Nov 2009 to 132.250.22.8. Redistribution subject to AIP license or copyright; see http://jap.aip.org/jap/copyright.jsp

eses for events occurring during the DSC ramps as follows. As the Ni/Si multilayers were heated, a temperature (~235 °C, see Fig. 2) was reached where interfacial reaction was initiated, resulting, as the temperature increased further, in the first exothermic energy release, followed by a second energy release peaking near the maximum ramp temperature of 560 °C. As detailed in Fig. 4, the intensity of these peaks varied inversely with increasing scan rate, such that the initial peak (peak 1), which was not detectable at the lowest scan rate, became the most intense peak at the highest scan rate. The second peak (peak 2) which was the most intense peak at the slowest scan rate, became undetectable at the highest scan rate. We associate peak 1 with exothermic Ni/Si mixing (rapid diffusion and/or melting) at the thermodynamically unstable Ni/Si interface, and peak 2 with secondary crystallization of Ni silicide phases. The competition between rapid diffusion/melting and crystallization/growth is influenced by the scan rate, such that the rapid process is more pronounced in the rapidly scanned materials, due to kinetic limitations on the crystallization rate of the secondary solid phases. If the rapid mixing process results from melting, it may be to some extent self-sustaining[16] at the highest scan rates where there is less thermal loss, since for the unstable Ni/Si interface, the exothermic energy associated with the negative enthalpy of mixing of Ni and Si greatly exceeds the endothermic effect associated with the disorder of melting. In the most rapidly scanned materials [Fig. 5(a)], complete intermixing of Ni and Si occurred, apparently with nearly simultaneous crystallization, since only one discernible exothermic peak was observed. The fundamental question relates to the origin of the rapid mixing process: melting versus rapid diffusion by a short circuit mechanism such as grain boundary diffusion.

B. Metastable melting

The possibility of metastable melting in the rapidly scanned sample can be further evaluated by means of a thermodynamic analysis of the experimental Ni–Si phase diagram. For this purpose, we used THERMOCALC[15] for the thermodynamic calculations. The calculations were completed using the thermodynamic descriptions of Tokunaga *et al.*,[17] in which the Gibbs energies of the disordered phases (liquid, fcc Ni solid solution) were modeled as regular solutions with Redlich–Kister interaction parameters fitted to the experimental data. For the ordered fcc Ni phase, an additional contribution to the Gibbs energy associated with ordering was modeled with two sublattices. For the stoichiometric phases appearing in the Ni–Si phase diagram (including Ni_3Si and $NiSi_2$), Gibbs energies were calculated from the weighted energies of the pure end members combined with an empirical term to fit the experimental data. The resulting equations of state allowed the calculation of metastable equilibria among any combination of Ni–Si phases over a wide range of temperatures.

In Fig. 6(a), the complete Ni–Si diagram calculated with the optimized parameters of Tokunaga *et al.*[17] is presented; the diagram contains 11 distinct phases. In Fig. 6(b) we show the results of calculating metastable equilibria among just three of the phases: the pure Ni and Si end members, and the liquid phase. This scenario corresponds to the situation of ultrarapid heating where there is no time for growth of intermediate crystalline phases, only formation of a melt. The phase diagram of Fig. 6(b) indicates a deep trough of metastable liquid extending to low temperatures, and centered at approximate composition 0.33 mol fraction Si. This metastable liquid encompasses (fortuitously) the bulk composition chosen for the multilayer films (0.35 mol fraction Si), giving credence to the possibility of extensive metastable melting for the rapidly heated multilayers. In Fig. 6(c) we calculated metastable equilibria with one additional phase: the ordered fcc solid solution. The presence of the ordered solid solution phase significantly reduces the region available for metastable melting and the minimum melting temperature is raised to 400 °C.

C. Solid state diffusion

If only solid state diffusion is considered without melting, the complete homogenization of the rapidly heated multilayers relative to the remnant layering of the slowly heated samples is counterintuitive. Nonetheless, it is useful to consider diffusion from a more quantitative perspective. Assuming a composition-independent diffusivity, the Fickian diffusion formalism

$$\frac{\partial C}{\partial t} = D\frac{\partial^2 C}{\partial x^2},$$

where C is the concentration of Ni, x is the distance, and t is time, with boundary conditions

$$x=0 \quad \text{and} \quad x=L: \frac{\partial C}{\partial x}=0,$$

and initial conditions

$$t=0: C=kC_0,$$

where

$$k=0(x<L/2), \quad k=1(x\geq L/2)$$

can be solved numerically using an error function solution to give concentration profiles approximating the expected Ni and Si distribution at 560 °C as a function of time. For these calculations we assumed that the Ni diffusion relative to Si is the more rapid process. Since the sputtered films are granular, we also assumed that grain boundary diffusion is the dominant mass transport mechanism. During reactive diffusion, the diffusivities of Ni through the product phases must be considered. Literature data are few, but representative grain boundary diffusivity [D(gb)] values in different matrices are summarized in Table I, where it can be seen that values vary widely.

Specifically, the difference between Ni transport in $NiSi_2$ versus Ni_2Si is about six orders of magnitude, which would have an extreme effect on the calculated concentration profiles at the Ni/Si interface. In Fig. 7, we show a diffusion profile calculated with D(gb) for Ni/$NiSi_2$. The Ni mass transport is represented in the figure by C/C_0, the ratio of the Ni concentration after a scan to the concentration before the

Downloaded 24 Nov 2009 to 132.250.22.8. Redistribution subject to AIP license or copyright; see http://jap.aip.org/jap/copyright.jsp

FIG. 6. (Color online) (a) Calculated Ni–Si equilibrium phase diagram. (b) Diagram assuming metastable equilibria among the pure Ni and Si end members and the liquid phase. (c) Metastable equilibria among Ni solid solution, Si, ordered fcc phase, and liquid. (d) Metastable equilibria among pure Ni and Si end members, Ni_3Si, $NiSi_2$, and liquid.

scan shown as a function of the distance from the interface. The calculation shown by the solid line in Fig. 7 corresponds to the approximate time at 560 °C which would result from a 16 000 °C/s scan. For this situation, the diffusion is limited to a region of less than 2 nm at the interface. The dashed line in Fig. 7 shows a profile calculated for a 120 °C/s scan, where the predicted mass transport is similar to that observed in Fig. 5(b). Significant transport of Ni has occurred throughout the 20 nm extent depicted in the model, yet homogenization has not occurred. If the D(gb) value for Ni in Ni_2Si or the generalized value for Ni diffusivity in a metal matrix are used, essentially complete homogenization results for both scan rates. Thus, different diffusivities are required to explain the results of slow versus rapid scan rates. This suggests an active role of $NiSi_2$ at the slow scan rates and increased influence of other phases such as metastable liquid or

TABLE I. Relevant diffusivities at 560 °C.

Species/Matrix	D(gb) (m^2/s)	Reference
$Ni/NiSi_2$	3.9×10^{-18}	18
Ni/Ni_2Si	$\sim5\times10^{-12}$	19
Ni/metal (avg.)	5×10^{-14}	20

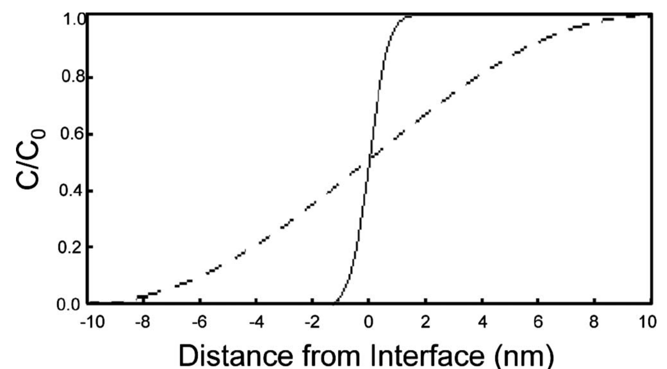

FIG. 7. Diffusion profile calculated with D(gb) for $Ni/NiSi_2$. Solid line represents calculation for a 16 000 °C/s scan, and dashed line is for a 120 °C/s scan. C/C_0 is the ratio of the Ni concentration after a temperature scan to the concentration before the scan.

Downloaded 24 Nov 2009 to 132.250.22.8. Redistribution subject to AIP license or copyright; see http://jap.aip.org/jap/copyright.jsp

glass, or Ni-rich silicides (e.g., Ni_3Si) with higher diffusivities at the rapid scan rates. We know from SAED and XRD that $NiSi_2$ and Ni_3Si are major product phases for both scan rates. The compositional layering evident in Figs. 5(d) and 5(e) could be explained by the influence of an $NiSi_2$-rich layer, which would serve as an effective diffusion barrier, preventing further homogenization in the slow scans. The lack of layering in Fig. 5(a), together with the diffraction data implies interspersed Ni_3Si and $NiSi_2$ in the rapid scan products. It seems unlikely on microstructural grounds that a completely interspersed, relatively uniform texture would result from interfacial mass transport in the solid state, since there has to be a continuous directional component to the mass flux and associated reaction. An efficient homogenization process seems to be required, for which melting provides the most probable explanation.

D. Effect of scan rate on reaction energetics

It is useful to compare the observed enthalpies (Fig. 4) with the values computed[21] for complete reaction to Ni_2Si and NiSi [the equilibrium products predicted by Fig. 6(a) for 0.35 mol fraction Si] versus reaction to the observed products (Ni_3Si and $NiSi_2$). Our calculations suggest 8.9 μJ for the equilibrium reaction and 8.3 μJ for our observed products. The maximum value observed at the most rapid scan rates in Fig. 4, i.e., 9.8 μJ, is higher than the maximum predicted for the equilibrium phase assemblage. We attribute this to added energies associated with the amorphous to crystalline transition in Si, and to spontaneous grain growth in Ni. With these caviats, the DSC data appear to be in reasonable agreement (within 15%) of predicted values.

The fine structure of peak 1 revealed in Fig. 3 suggests the need for further interpretation. For example, it is possible that a small amount of melting (the first maximum of the doublet of peak 1) occurs even in the slow scans, but that this melting gives way to crystallization (e.g., $NiSi_2$) (the second maximum of the doublet), that impedes further melting and homogenization. As the scan rate increases, the time available for $NiSi_2$ to form is less, so that the amount of melting increases, resulting in a diminished doublet. At the highest scan rate, melting and complete homogenization occur simultaneously with the crystallization of Ni_3Si and $NiSi_2$ products, resulting in a combination of peaks 1 and 2.

V. CONCLUSIONS

In summary, we favor the application of a metastable melting hypothesis to explain the enhanced mass transport and microstructure produced by the ultrarapid heating of the Ni/Si multilayers (DSC scan rate 16 000 °C/s), whereas we postulate that solid state diffusion is responsible for the microstructure produced by the slow scan rate (120 °C/s). Our observations and conclusions regarding the reactions to form the silicide phases Ni_3Si and $NiSi_2$ as final reaction products appear to be consistent with the DSC enthalpies, and the relatively low grain boundary diffusivity of $NiSi_2$. These results point to the possibility of alternative routes for practical processing of semiconductor silicide interconnects under conditions of flash annealing. Further combined microstructural/nano-DSC experiments will provide more details on the potential use of ultrarapid heating in Si-based device fabrication.

[1] Semiconductor Industry Association, International Technology Roadmap for Semiconductors: Semiconductors 2007 Edition Front End Processes, pp. 29 and 30, 181 Metro Drive, Suite 450 San Jose, CA 95110, http://public.itrs.net.

[2] E. P. Gusev, V. Narayanan, and M. M. Frank, IBM J. Res. Dev. **50**, 387 (2006).

[3] W. J. Lee, D. W. Kim, S. Y. Oh, Y. J. Kim, Y. Y. Zhang, Z. Zhong, S. G. Li, S. Y. Jung, I. S. Han, T. K. Gu, T. S. Bae, G. W. Lee, J. S. Wang, and H. D. Lee, J. Appl. Phys. **101**, 103710 (2007).

[4] N. Biswas, J. Gurganus, and V. Misra, Appl. Phys. Lett. **87**, 171908 (2005).

[5] C. Rivero, P. Gergaud, M. Gailhanou, O. Thomas, B. Froment, H. Jaouen, and V. Carron, Appl. Phys. Lett. **87**, 041904 (2005).

[6] J. A. Kittl, M. A. Pawlak, C. Torregiani, A. Lauwers, C. Demeurisse, C. Vrancken, P. P. Absil, and S. Biesemans, Appl. Phys. Lett. **91**, 172108 (2007).

[7] R. Lindsay, B. Pawlak, J. Kittl, K. Henson, C. Torregiani, S. Giangrandi, R. Surdeanu, W. Vandervorst, A. Mayur, J. Ross, S. McCoy, J. Gelpey, K. Elliott, X. Pages, A. Satta, A. Lauwers, P. Stolk, and K. Maex, Mat. Res. Soc. Symp. Proc. **765**, D7.4.1 (2003).

[8] W. Skorupa, W. Anwanda, D. Panknina, M. Voelskowa, R. A. Yankova, and T. Gebel, Vacuum **78**, 673 (2005).

[9] B. Adams, D. Jennings, K. Ma, A. J. Mayur, S. Moffatt, S. G. Nagy, and V. Parihar, Proceedings of the 15th IEEE International Conference on Advanced Thermal Processing of Semiconductors, Catania, Italy, 2007 (unpublished), pp. 155–160.

[10] Y. Setiawan, P. S. Lee, and K. L. Pey, Appl. Phys. Lett. **88**, 113108 (2006).

[11] S. E. Thompson and S. Parthasarathy, Mater. Today **9**, 20 (2006).

[12] F. Nemouchi, D. Mangelinck, C. Bergman, and P. Gas, Appl. Phys. Lett. **86**, 041903 (2005).

[13] L. A. Clevenger, C. V. Thompson, R. C. Cammarata, and K. N. Tu, Appl. Phys. Lett. **52**, 795 (1988).

[14] R. E. Cavicchi, G. E. Poirier, N. H. Tea, M. Alfridi, D. Berning, A. Hefner, J. Suehle, M. Gaitan, S. Semancik, and C. Montgomery, Sens. Actuators B **97**, 22 (2004).

[15] Certain commercial equipment, instruments, or materials are identified in this document. Such identification does not imply recommendation or endorsement by the National Institute of Standards and Technology, nor does it imply that the products identified are necessarily the best available for the purpose.

[16] L. A. Clevenger, C. V. Thompson, and K. N. Tu, J. Appl. Phys. **67**, 2894 (1990).

[17] T. Tokunaga, K. Nishio, H. Ohtani, and M. Hasebe, CALPHAD: Comput. Coupling Phase Diagrams Thermochem. **27**, 161 (2003).

[18] C. Hayzelden and J. L. Batstone, J. Appl. Phys. **73**, 8279 (1993).

[19] W. Losch and W. Acchar, Phys. Status Solidi A **173**, 275 (1999).

[20] A. M. Brown and M. F. Ashby, Acta Metall. **28**, 1085 (1980).

[21] C. W. Bale, P. Chartrand, S. A. Degterov, G. Erikkson, K. Hack, R. Ben Mahfoud, J. Melancon, A. G. Pelton, and S. Peterson, CALPHAD: Comput. Coupling Phase Diagrams Thermochem. **26**, 189 (2002).

Downloaded 24 Nov 2009 to 132.250.22.8. Redistribution subject to AIP license or copyright; see http://jap.aip.org/jap/copyright.jsp